

Contents lists available at ScienceDirect

# Acta Materialia

journal homepage: www.elsevier.com/locate/actamat



# An atomistic-to-microscale computational analysis of the dislocation pileup-induced local stresses near an interface in plastically deformed two-phase materials



Yipeng Peng<sup>a</sup>, Rigelesaiyin Ji<sup>a</sup>, Thanh Phan<sup>a</sup>, Wei Gao<sup>b</sup>, Valery I. Levitas<sup>a,c,d</sup>, Liming Xiong<sup>a,\*</sup>

- <sup>a</sup> Department of Aerospace Engineering, Iowa State University, Ames, IA 50011, USA
- <sup>b</sup> Department of Mechanical Engineering, University of Texas at San Antonio, TX 78249, USA
- <sup>c</sup> Department of Mechanical Engineering, Iowa State University, Ames, IA 50011, USA
- <sup>d</sup> U.S. Department of Energy, Ames Laboratory, Ames, IA 50011, USA

### ARTICLE INFO

### Article history: Received 11 June 2021 Revised 12 November 2021 Accepted 13 January 2022 Available online 15 January 2022

Keywords:
Dislocation pileup
Material interface
Stress concentration
Eshelby model
Molecular dynamics
Multiscale modeling

### ABSTRACT

Taking the two-phase material as a model system, here we perform atomistic-to-microscale computational analysis on how the dislocations pileup is formed at a buried interface through two-dimensional concurrent atomistic-continuum simulations. One novelty here is a simultaneous resolution of the  $\mu$ m-level dislocation slip, the pileup-induced stress complexity, and the atomic-level interface structure evolution all in one single model. Our main findings are: (i) the internal stresses induced by a pileup spans a range up to hundreds of nanometers when tens of dislocations participate the pileup; (ii) the resulting stress concentration decays as a function of the distance, r, away from the pileup tip, but deviates from the Eshelby model-based  $1/r^{0.5}$ , where the interface was assumed to be rigid without allowing any local structure reconstruction; and (iii) the stress intensity factor at a pileup tip is linearly proportional to the dislocation density nearby the interface only when a few dislocations are involved in the pileup, but will suddenly "upper bend" to a very high level when tens of or more dislocations arrive at the interface. The gained knowledge can be used to understand how the local stresses may dictate the plastic flow-induced phase transformations, twinning, or cracking in heterogeneous materials such as polycrystalline steel, Ti-, Mg-, high entropy alloys, fcc/bcc, fcc/hcp, and bcc/hcp composites, containing a high density of interfaces.

© 2022 Acta Materialia Inc. Published by Elsevier Ltd. All rights reserved.

### 1. Introduction

The microstructure of many engineering materials is usually heterogeneous in nature due to the presence of a high density of interfaces, such as grain boundaries (GBs), phase boundaries (PBs), stacking faults, or twin boundaries (TBs), etc. When these materials are subjected to a plastic deformation, the interactions between those interfaces and the plasticity carriers, e.g., dislocations, control their microstructure evolution and overall performance. A pileup forms when the interface blocks the slip containing a queue of dislocations. The dislocation pileup leads to a local strain accumulation and a stress concentration, i.e., a stress magnitude at a fraction of theoretical strength ahead of the spearhead of a pileup [1–3]. Even at moderate applied stresses, the stress concentration factor at a pileup tip can be as large as 10 to 100 [4–6]. If such a

E-mail address: lmxiong@iastate.edu (L. Xiong).

high local stress cannot be fully relieved by dislocation cross-slip, transmission, the other structure changes such as phase transformations (PTs), crack initiations, twinning, and even atomic diffusion will then occur.

In the past decades, extensive experimental research efforts have been dedicated to characterizing the complex stress field induced by a slip-interface reaction across a variety of different length scales. For instance, at the microscale, the electron backscattered diffraction (EBSD) or high-resolution EBSD (HR-EBSD) has been widely used to measure the strain accumulation at the slip-GB intersection [1,2,4,7]. At the nanoscale, the transmission electron microscopy (TEM) or high-resolution TEM (HR-TEM) is usually deployed [8–13] to resolve the detailed dislocation activities near the GBs. These experiments have, of course, largely advanced the researchers' understanding in this field but are limited in several aspects: (i) the local internal stresses are usually not directly measured in experiments. Instead, they are calculated from the EBSD-/TEM-measured strain using certain constitutive rules, e.g.,

<sup>\*</sup> Corresponding author.

the Hooke's law, in elasticity or higher-order theories; and (ii) the existing experimental techniques have a limited time-scale resolution, at which the capture of the local structure change, such as the dislocation transmission or step formation process at the GB, during the dislocation piling up process is non-trivial. Up to date, it remains difficult using single-scale techniques to simultaneously resolve the configuration of tens of or more dislocations piling up at the interface, the µm-level stress concentration ahead of the pileup tip, as well as the atomic-scale structure evolution at the slip-interface intersection. These limitations lead to a series of unanswered questions: is it possible to directly quantify the internal stress around the dislocation-interface intersection instead of measuring the strain and then converting it into stresses according to the theory of elasticity? If it is, how will such a directly measured local stress differ from the prediction by classical models, such as the Eshelby model, at the continuum level? Can we quantitatively correlate the density of the dislocations in a localized slip with the internal stress intensity factor ahead of the slip-interface intersection? If yes, at what length scales? Clearly, a seek of the answers to those questions remains challenging from the experimental point of view.

High-fidelity computer simulations are thus essential to avoid interpreting the experimental results using assumed theories or mechanisms. With the advent of high-performance computing, molecular dynamics (MD) have become a powerful tool for studying materials' deformation behavior at an atomistic resolution. The equations in MD are discretized in time and do not involve spatial derivatives. It, consequently, possesses no barrier in simulating dislocations slip and the local structural change. Thus, MD simulations can unravel the mechanisms underlying the material's constitutive behavior and may correlate the fine-scale interface structure changes with the behavior of materials at a larger length scale. However, by considering the materials as a collection of atoms, MD simulations is computationally demanding. If only a modest computational resource is used, the length scale of an MD model is usually limited at the nanoscale and even below if a sophisticated interatomic potential is deployed. This limitation prevents MD from being used to fully reproduce the material's deformation behavior observed in real experiments. As far as the slip-interface reactions are concerned, in many existing MD models, one single [14,15] or only a few dislocations are introduced close to an interface in a simulation cell with a very limited volume [16-18]. As such, the dislocation density becomes unrealistically high. Also, the forces induced by the interaction between periodic images are non-negligible and may pollute the results [18,19]. It thus casts doubt on directly mapping the nanoscale MDsimulation-based mechanisms to the microscale experimental observation for a dislocation-interface reaction [20]. Historically, to scale up in length, continuum models enjoy the most popularity in understanding the deformation behavior of materials at large length scales. In particular, for heterogeneous materials containing interfaces, a variety of continuum models [21-24], such as dislocation dynamics (DD), crystal plasticity finite element (CPFE), or phase field approach (PFA), have been developed. In particular, the interaction between dislocation pileups and the GBs leading to slip transfer [25] and PTs [26,27] in materials under compression and shear have been studied with PFA. Without the explicit description of the atomistic structure of dislocation/interfaces, these continuum approaches provide researchers with a considerable gain in computational efficiency comparing with MD. Nevertheless, they require constitutive rules as inputs, which usually need to be carefully calibrated from experiments and fine-scale simulations. This is, however, not trivial, especially when describing the interaction between dislocation-mediated plastic flow and the buried interface becomes essential. Understanding the dislocation-interface reaction in materials thus necessitates multiscale simulations to overcome many limitations in continuum and also fully atomistic models

In this work, a concurrent atomistic-continuum (CAC) approach [28-39] built upon a formulation [40-42] that unifies the atomistic and continuum description of materials within one framework is deployed. Here, as a first demonstration of the CAC's applicability in characterizing the local stress complexity induced by a micrometer-level dislocation pileup at an atomically-resolved interface, a two-dimensional (2D) two-phase material (the hexagonal and square phases co-exist with an incoherent interface in between) under a well-controlled plastic shear is selected as a model system. We choose such a simple system as a model material because: (i) the dislocation pileup at the GBs and the pileup-induced local stresses in many realistic 2D materials, such as boron nitride [43], colloidal crystals [44], MoTe<sub>2</sub> [45] and so on, significantly contribute to their deformation behavior (PT in particular) but is not fully understood up to date; (ii) the 2D model setup under a plane strain condition provides us with an opportunity to validate the simulation results through comparing them with the analytical solutions from the plane elasticity theory-based Eshelby model [46]; and (iii) if desired, the interface structure in this system can be easily tuned to approximate the realistic interface in recently developed high-performance hcp/fcc, hcp/bcc, or fcc/bcc metallic composites, such as Ti/Al [47], Mg/Nb [48], Cu/Nb [49], and among several others.

This paper is organized as follows. In Section 2, we briefly review and introduce the CAC methodology, the model material, the computer model set-up, as well as the boundary and loading conditions. The results from the microscale CAC together with nanoscale MD simulations of the dislocation pileup at the interface and the pileup-induced stress concentration are then analyzed in Section 3. Thereafter, this work is concluded with a summary of our major findings as well as a discussion of future research in Section 4

### 2. Methodology and the computer model setup

The CAC methodology is derived from the numerical implementation of a formulation in [41,50-52], which is a generalization of the Irving-Kirkwood procedure [53-56] in statistical mechanics. It views the solid material as a collection of lattice cells continuously distributed in space, within each of which a group of discrete atoms is embedded. The continuum-level physical quantities, including mass density, linear momentum density, energy density, momentum flux (also referred as stress in continuum mechanics), and energy flux, are then defined from the atomic positions, velocities, and interatomic forces through Dirac or Gaussian distribution functions [40,42]. An introduction of these physical quantities into the classical Newtonian mechanics leads to a series of equations, i.e., mass conservation, momentum balance, and energy conservation equations, which can govern the mechanical, thermal, and mass transport behavior of materials from the bottom up [41]. These equations are partial differential equations in the same form as the balance equations in classical continuum mechanics but with atomistic information built-in. Thus, those equations can be solved using numerical techniques, such as finite-difference or finite element (FE), which are commonly used for solving the equations in continuum mechanics.

As an FE implementation [38,39] of the atomistic field formulation, CAC has several unique features: (1) unlike the FE model in classical continuum mechanics considering the material as a collection of mass points without any internal structures, each FE node in CAC is one lattice cell containing a group of atoms whose motions are independent from each other; (2) the material behavior in the atomistic and CG domains of a CAC model is governed by the same constitutive rule, i.e., the interatomic potential. In partic-

**Table 1**The parameters of the modified L-J potential for both the square and hexagonal phases.

mass (g/mole)	σ (Å)	$\varepsilon$ (eV)	H (eV·Å)	$r_{mh}$ (Å)	$\sigma_h$ (Å)	cut-off (Å)
63.546	2.277	0.415	-0.4964	3.6432	0.4772	5.0094

ular, the forces acting on the atoms within each FE node in the CG domain are calculated by converting the interatomic forces into the internal force density through the deployment of a Gauss quadrature scheme [38,39]; (3) it does not need any special treatments to describe discontinuity, such as dislocations or cracking, at the continuum level because the slip systems as well as the cleavage planes are all built in; (4) the dislocations can be also initially introduced into the CG domain by displacing the FE nodes according to the dislocation-induced displacement field derived from the theory of elasticity[7]. This differs from other continuum approaches which accommodate dislocations through the deployment of either a contact model in [57,58], a Heaviside step function in [59], or an additional DOF in CPFE [60,61]; (5) it does not need sophisticated rules for passing the dislocation-mediated plastic flow from the continuum domain to the atomistic domain and vice versa [28-30]; (6) the CG domain in CAC has a significantly less degrees of freedom (DOF) than that in a fully atomistic model. It may be scaled up to the micrometer level and in turn, enable us to model the pileup of tens of dislocations at an interface. This goes beyond the reach of a traditional MD model because MD usually has a limited length scale at nanometers and can only accommodate several dislocations in an equilibrium pileup [18]. Furnished with the above features, CAC have been applied to simulate: (a) dislocations in Cu, Al, Ni, and Si by CAC using rhombohedral-shaped elements with the element boundaries being aligned on the slip plane [31]; (b) Si-I  $\rightarrow$  Si-II PT in single-crystal Si by CAC [39]; and (c) the dislocation pile up at a grain boundary (GB) as well as the subsequent dislocation transmission across the GB, in bi-crystalline Cu [30]. These results confirm that CAC has a predictive capability at approximately the same level as that of MD but demands significantly less computational resources. It thus provides us with an ideal platform for understanding the micrometer-level dislocation pileup at a material interface, the atomic-level interface structure evolution, together with the subsequent phase transformation and twinning, if there would be any.

For the two-dimensional two-phase material system under consideration here, two phases (hexagonal and square) co-exist with an interface in between. The interaction between the atoms in both the square and hexagonal phases is described using a modified Lennard-Jones (L-J) potential as shown in Eq. (1) by Lee and Ray [62]:

$$V_{MLJ} = -4\varepsilon \left[ \left( \frac{\sigma}{r} \right)^6 - \left( \frac{\sigma}{r} \right)^{12} \right] - \frac{H}{\sigma_h \sqrt{2\pi}} e^{\left[ -\frac{(r - r_{mh})^2}{2\sigma_h^2} \right]},\tag{1}$$

which was originally proposed to study the bcc-to-hcp PT in iron.

The modified L-J potential's functional form in Eq. (1) is the combination of a traditional L-J (12-6) term and an inverse Gaussian term. The 12-6 term leads to a stable hexagonal crystal structure at zero stress. The addition of an inverse Gaussian into the modified L-J potential gives rise to a square lattice structure. Here the parameters H,  $r_{mh}$ , and  $\sigma_h$  in Eq. (1) were chosen to stabilize: (i) an immobile but deformable incoherent interface between the square and the hexagonal phase, which can act as the obstacles to dislocation motion; and (ii) the core structure of a dislocation in the hexagonal phase. The interatomic potential parameters satisfying these two conditions are listed in Table 1. Fig. 1 a and 1 b shows the corresponding potential energy landscapes and the cells

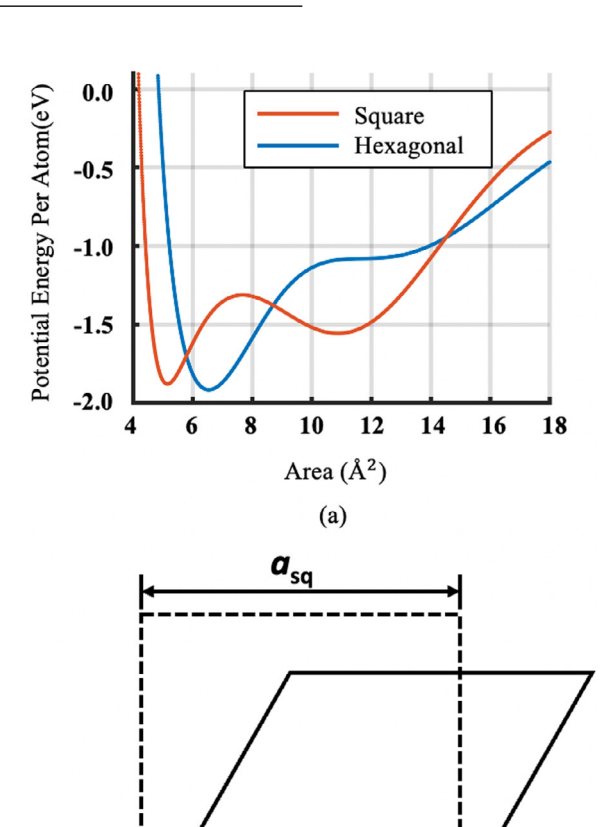


**Fig. 1.** (a) The potential energy of the square (blue) and hexagonal (brown) lattices by a modified Lennard-Jones form in Eq. (1) and (b) the unit cell transformation from square to hexagonal phase.

 $a_{\mathsf{hex}}$ 

(b)

of these two phases with their lattice constants being noted as  $a_{\rm sq}$  and  $a_{\rm hex}$ .

The 2D CAC model for the two-phase material with square and hexagonal lattices coexisting is then constructed (Fig. 2 a). The material on the right side of the interface is in a square phase and has a dimension of  $L_{x-sq}$  along the x-direction. By contrast, the material domain on the left side of interface is in a hexagonal phase and has a dimension of  $L_{x-hex}$  along the x-direction. The sample dimension along the y-direction is chosen as  $L_y = m_{\text{hex}} a_{\text{hex}} = n_{\text{sq}} a_{\text{sq}}$ , where  $m_{\text{hex}}$  and  $n_{\text{sq}}$  are the numbers of the hexagonal and square lattice cells along the y direction,  $a_{\rm hex} = 2.41$  Å and  $a_{\rm sq} = 2.56$  Å are the lattice constants for the hexagonal and square lattice, respectively. For the hexagonal phase on the left side of the interface, the material domain is in a CG description and is discretized into coarse FEs. Each FE, the center of which is indicated as green squares in Fig. 2 b, contains 64 atoms. Due to the deployment of a CG description,  $L_{x-\text{hex}}$  can be scaled up to the micrometer level and even above. Most importantly, these FEs can slide with each

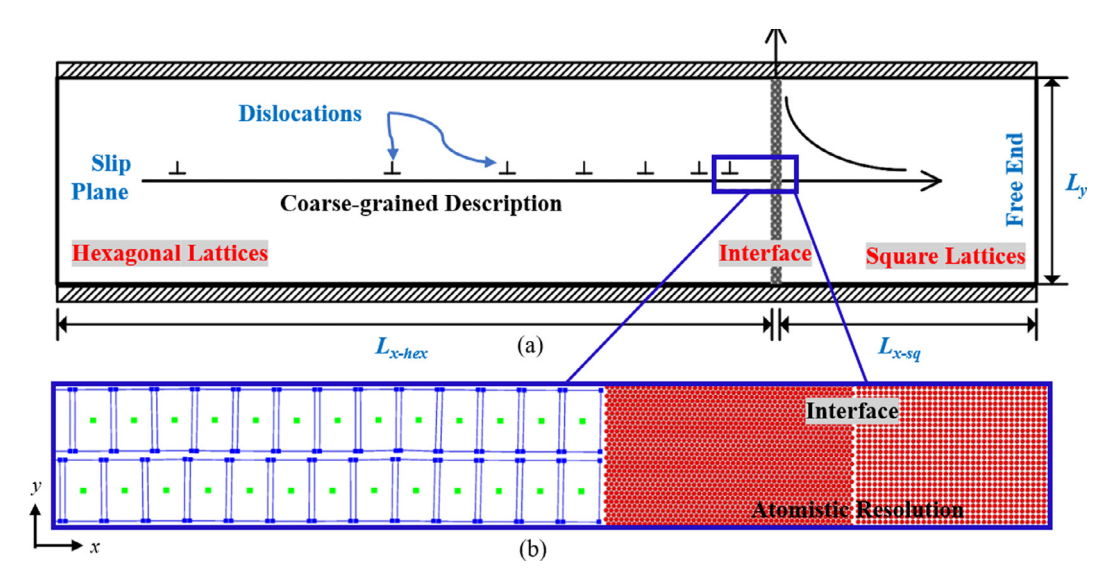


Fig. 2. The CAC model set-up for the dislocation pileup at an interface in the two-phase system: (a) the CG description of dislocations in hexagonal lattice away from the interface and the atomistic resolution near the interface; (b) a zoom-in display of the region in the dashed box of (a).

other along the element boundaries, which are currently aligned with one of the slip planes, to accommodate the dislocation migrations along the [100] direction without the need of tracking the motion of each atom in the hexagonal phase. In details, a queue of dislocations can be initially introduced into the CG domain one by one through displacing the FE nodes there according to the the solution from the theory of elasticity for the displacement of a dislocation. Here, the dislocation nearest the interface is labeled as "1", the dislocation second nearest the interface is labeled as "2", so on and so forth. Such a dislocation indexing strategy does not change on the fly of the simulations and has been used in the analysis of our simulation results to be discussed in the following sections.

Different from the above CG description of the dislocations away from the interface, the material domain near the interface is resolved at a fully atomistic resolution (Fig. 2 a) because the deformation behavior at the interface is critical and will dictate its overall constitutive response. As indicated by the crystallographic orientations of the hexagonal and square phases being in Fig. 2 b, an incoherent interface has been carefully designed here such that: (i) the dislocation-mediated slip in the hexagonal phase is perpendicular to the interface; and (ii) the dislocation transmission or slip transfer will be discouraged the most (the evidence why the slip transfer across this interface is unfavorable can be found through Schmid factor, geometric compatibility factor, and also the Burgers vector analysis as shown in Section 3.1). In this way, the pileup-induced stress field can be well quantified without the need of considering many other complexities caused by the slipinterface inclined angles, dislocation transmission, cross-slip, and so on. However, it should be noted that, among all the possible interfaces, the constructed interface satisfying the above two conditions is not the one with an energy minimum, although our analysis on the slip-interface reaction will indeed benefit from such a setup.

Thereafter the introduction of a queue of dislocations and the construction of the carefully designed interface, the formation of a pileup can be then simulated through the following steps: (1) First of all, the displacement along z direction of the sample is constrained to achieve a plane strain condition, which is consistent with the setup in the classical Eshelby model [46]; (2) The model containing the initially introduced dislocations is equilibrated for a duration of 20 ps with a timestep of 1 fs to achieve an equilibrium configuration of dislocations; (3) A homogeneous shear strain

of  $\varepsilon_{xy} = 2 \times 10^{-4}$  is then imposed. This is in turn, followed by an equilibration for a duration of 1 ps with the upper and bottom boundaries being fixed. The strain rate resulting from such a loading strategy is thus at a level of  $2 \times 10^8$  /s, which is at the same level as that in common MD simulations. It should be noted that, although the material is deformed at a level of orders of magnitude of higher than that in experiments, the pileup-induced stress is only characterized here when the system is fully equilibrated at a desired shear; (4) This procedure repeats until the averaged shear stress of the whole model arrives at a desired level noted as  $\tau_{ap}$ . This is realized through monitoring the shear stress when the shear strain has been imposed. If the shear stress is below the desired  $\tau_{ap}$ , the shear strain will continue increasing. If the shear stress is above the desired  $\tau_{ap}$ , the imposed shear strain will be adjusted to a lower level. When  $\tau_{ap}$  arrives at the desired value, the top and bottom boundaries of the sample will be constrained and not allowed to move any further along both x and y directions; (5) The  $\tau_{ap}$  will then drive dislocations to migrate towards the interface. For the sample under different  $\tau_{ap}$ , the dislocation configurations will largely differ from each other: the higher the applied shear, the smaller spacing between dislocations. In this way, the dislocation pileup will be formed and in turn a stress concentration ahead of the pileup tip will be generated. The level of this stress concentration can be then related with the number of the dislocations participating the pileup, the density of the dislocations behind the pileup tip, and of course, the level of the applied shear (see more details in Section 3).

Other than the microscale CAC model, a series of nanoscale fully MD simulations is also performed using LAMMPS [63] for validation purpose. The dimensions, and the number of DOF, and the computational cost for both the nanoscale MD and the microscale CAC models are listed Table 2.

The timescale of each simulation in the above table depends on the number of the dislocations in a pileup, i.e., the more dislocations, the longer run. Taking one CAC simulation containing 16 dislocations as an example, after 9 dislocations arrive at the interface within a duration of 0.4 ns, the CAC model has been equilibrated under a constant shear for another 1.6 ns. The resulting timescale of this run is 2 ns. The computational cost of such simulations are reasonably affordable because one such simulation only takes 72 h to finish if 96 computing cores on Comet of XSEDE are deployed. Given the perfectly linear scalability of our massively parallelized

**Table 2**The dimensions and the number of the DOF in MD and CAC models.

	$L_{x-hex}$	$L_{x-sq}$	Ly	DOF	Number of dislo- cations in a pileup	timestep/ second
Nanoscale MD Microscale CAC	420 nm 1.58 μm	70 nm 120 nm	84 nm 138 nm	1,355,284 atoms 315528 FE nodes +118392 atoms	0 ~ 8 5 ~ 16	170.034 54.283

The timestep/second is measured using compute node on COMET@SDSC with 96 cores.

**Table 3**The slip systems of the incoming and the potential outgoing dislocations as well as the resulting Schmid factors, the geometric compatibility factors.

Incoming slip system		Outgoing slip system		Metric value			
Slip plane	Slip direction	Slip plane	Slip direction	SF <sub>in</sub>	SF <sub>out</sub>	m′	$m'(SF_{in} + SF_{out})$
{001}  <sub>hex</sub> {001}  <sub>hex</sub> {001}  <sub>hex</sub>	(100)  <sub>hex</sub> (100)  <sub>hex</sub> (100)  <sub>hex</sub>	$\{01\} _{sq}$ $\{10\} _{sq}$ $\{10\} _{sq}$	$(10) _{sq}$ $(01) _{sq}$ $(0\bar{1}) _{sq}$	0.43 0.43 0.43	0.14 0.14 0.14	0.5 0 0	0.29 0 0

CAC simulator [64], for the formation of a longer pileup containing more dislocations within an even longer duration, e.g., 32 dislocations forming a pileup within 4 ns, one can still expect to finish the simulation within 72 h by using 384 computing cores.

#### 3. Simulation results

# 3.1. The Schmid factor, geometric compatibility factor, and burgers vector analysis

In order to confirm that the interface that we have constructed here indeed promotes the formation of a pileup by acting as a strong barrier to the dislocation-mediated slip, we have performed a series of detailed Schmid factor (SF), geometric compatibility factor (also noted as the Luster-Morris factor), and also the Burgers vector analysis as follows.

For the slip-transfer problem under consideration here, the incoming dislocations are in the hexagonal phase gliding on a {001} plane with a slip direction of (100), which can be noted as  $\{00\overline{1}\}(100)|_{\text{hex}}$ . The neighboring grain across the interface is in a square phase with three slip systems. If there would be any transmission across the interface, the outgoing dislocations will be in the {01} plane with a slip direction of (10), or in the {10} plane with a slip direction of (01), or in the {10} plane with a slip direction of  $(0\overline{1})$ , which are noted as  $\{01\}(10)|_{sq}$ ,  $\{10\}(01)|_{sq}$ , and  $\{10\}(0\overline{1})|_{sq}$ , respectively. For each of these three outgoing slip systems, with respect to the incoming dislocation slip system,  $\{00\overline{1}\}(100)|_{\text{hex}}$ , under a shear along x direction (See Fig. 2), the Schmid factors of the incoming and outgoing dislocations (noted as  $SF_{in}$  and  $SF_{out}$ ) are calculated and listed in Table 3. Moreover, the geometry compatibility factor, i.e., Luster-Morris parameter noted as  $m' = \cos(\phi)\cos(\kappa)$  [65] is also calculated and included in Table 3. Here,  $\phi$  is the angle between the slip direction of the dislocations in hexagonal and square phases,  $\kappa$  is the angle between the normal direction of the slip plane along which the dislocation glide in hexagonal and square phases. In addition to  $SF_{in}$ ,  $SF_{out}$  and m', a combined metrics proposed in a recent paper [66],  $m'(SF_{in} + SF_{out})$  is also calculated and included here.

Two major observations from Table 3 are: (1) if the geometric compatibility factor is used as a controlling metrics, the slip transfer and the outgoing dislocations can never happen through  $\{10\}(01)|_{sq}$  and  $\{10\}(0\bar{1})|_{sq}$  (the second and the third row of Table 3) because m'=0 for those two slip systems in square phases; (2) the slip transfer may occur through an outgoing dislocation along the  $\{01\}(10)|_{sq}$  in the square phase, the chance of which is, however, very low with m'=0.50 and  $m'(SF_{in}+SF_{out})=0.29$  (the first row of Table 3) because, according to the extensive

experimental data reported in [67-69], the threshold value of m' at which the slip transfer occurs is usually around 0.8 and even higher.

In order to confirm that the slip transfer indeed will not occur through an outgoing dislocation along the  $\{01\}(10)|_{sq}$  during the simulations, here we also perform a detailed Burgers vector analysis. Firstly, the interface that we have constructed can be viewed as a collection of dislocations resulting from the mismatch between hexagonal and square phases. Taking the square lattice as a reference, the Burgers vector of these resultant dislocations,  $\boldsymbol{b}_{res}$  [70–73], can be calculated as:

$$\{\boldsymbol{b}_{res}\} = \{\boldsymbol{t}_{sq}\} - \{\boldsymbol{P}\}\{\boldsymbol{t}_{hex}\},\tag{2}$$

where  $\{P\}$  is a transformation matrix for mapping the Miller index of a plane in hexagonal phases to that of a plane in square phases, which is  $\begin{pmatrix} 0.94 & -0.47 & -0.47 \\ 0.0 & 0.82 & -0.82 \end{pmatrix}$ . The column matrices  $\{t_{sq}\}$  and  $\{t_{hex}\}$  represent the Miller index of the interface in the square and hexagonal phase, respectively. According to the formula in [74,75], the transmission will occur as long as the deformation gradient, F, acting on the material which accommodates the outgoing dislocation, i.e., the square phase here, satisfies:

$$\{\boldsymbol{b}_{out}\} = (\boldsymbol{F}^{-1} - \boldsymbol{I}) \cdot \{\boldsymbol{p}\},\tag{3}$$

where  $\boldsymbol{b}_{out}$  is the Burgers vector of the outgoing dislocation. If it is along the slip system of  $\{01\}(10)|_{sq}$  in the square phase,  $\{\boldsymbol{b}_{out}\}=(1,0)^T$ ,  $\boldsymbol{I}$  is the identity matrix, and  $\boldsymbol{p}$  is the vector associated with the Burgers circuit of the defect in the interface.

When no dislocation arrives at the interface, p is simply the resultant Burgers vector, and is noted as  $\mathbf{p}_0 = \mathbf{b}_{res}$ , which can be calculated using Eq. (2) by using the  $t_{\rm sq}^0$  and  $t_{\rm hex}^0$  as indicated in Fig. 3 a. When the first dislocation arrives at the interface,  $\mathbf{p}_1 = \mathbf{b}_{in} + \mathbf{b}_{res}$ . During the pileup formation, for example, for the CAC model containing 16 dislocations, upon certain shear, 9 of them have arrived at the interface forming a step there, which will result in  $\mathbf{p}_9 = 9\mathbf{b}_{in} + 3\mathbf{b}_{res}$  since the step formed at the pileup tip occupies three atomic layers. In this scenario, the deformation gradient, F, required for producing of an outgoing dislocation of  $\boldsymbol{b}_{out} = (1,0)^T$  should satisfy  $\{\boldsymbol{b}_{out}\} = (\boldsymbol{F}^{-1} - \boldsymbol{I}) \cdot \{\boldsymbol{p}_9\}$ . According to  $\mathbf{E} = 1/2(F^TF - I)$ , the deformation gradient satisfying this equation will produce a shear strain of  $\gamma = 0.263$ . If the square phase is subjected to a shear strain at this level, a phase transformation (PT), rather than a slip, will occur because the square-to-hexagonal PT strain is  $\begin{pmatrix} -0.057 & 0.222 \\ 0.222 & -0.057 \end{pmatrix}$ . It also explains why we always observe the PT ahead of the pileup tip when more dislocations are

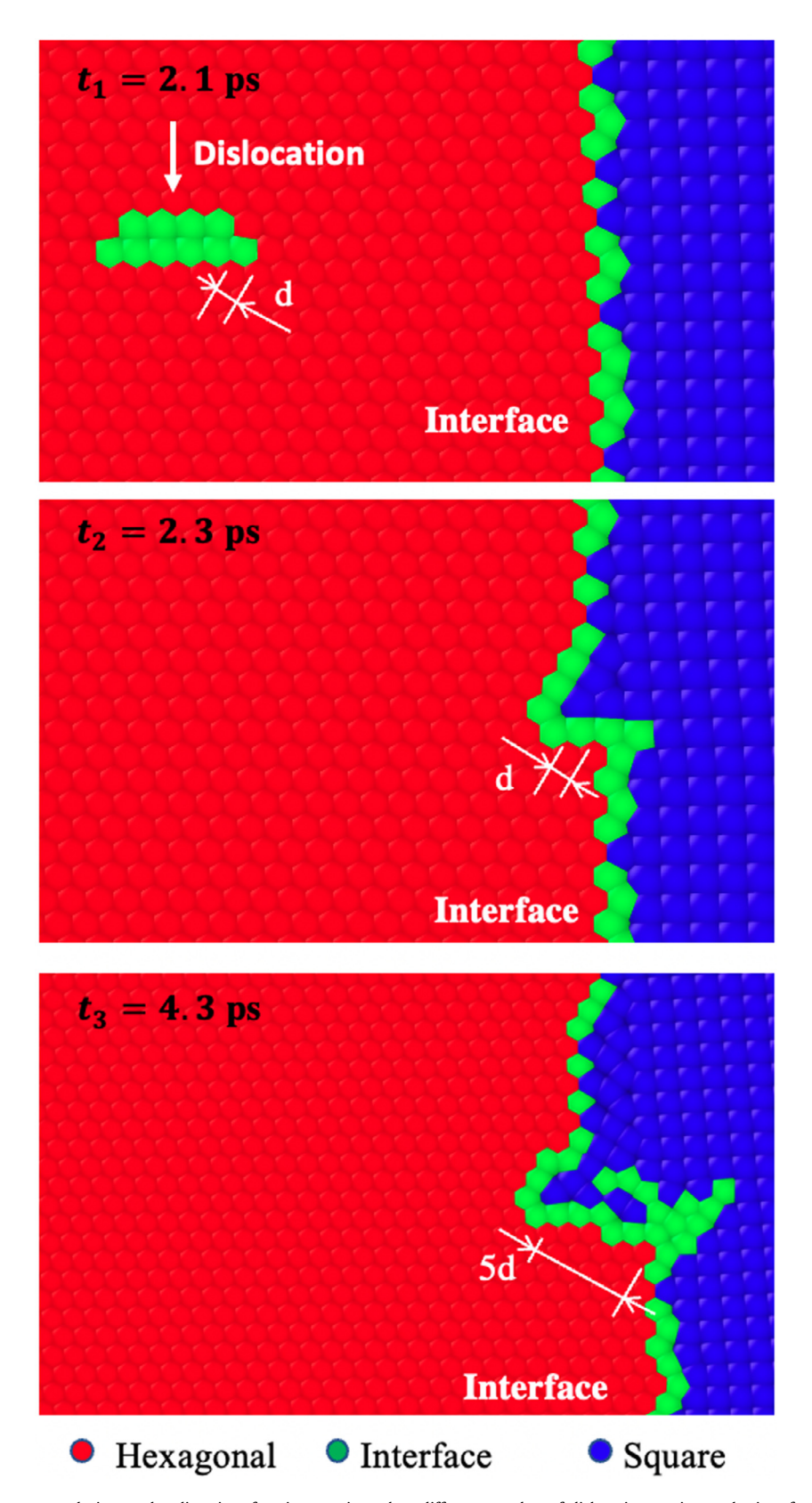
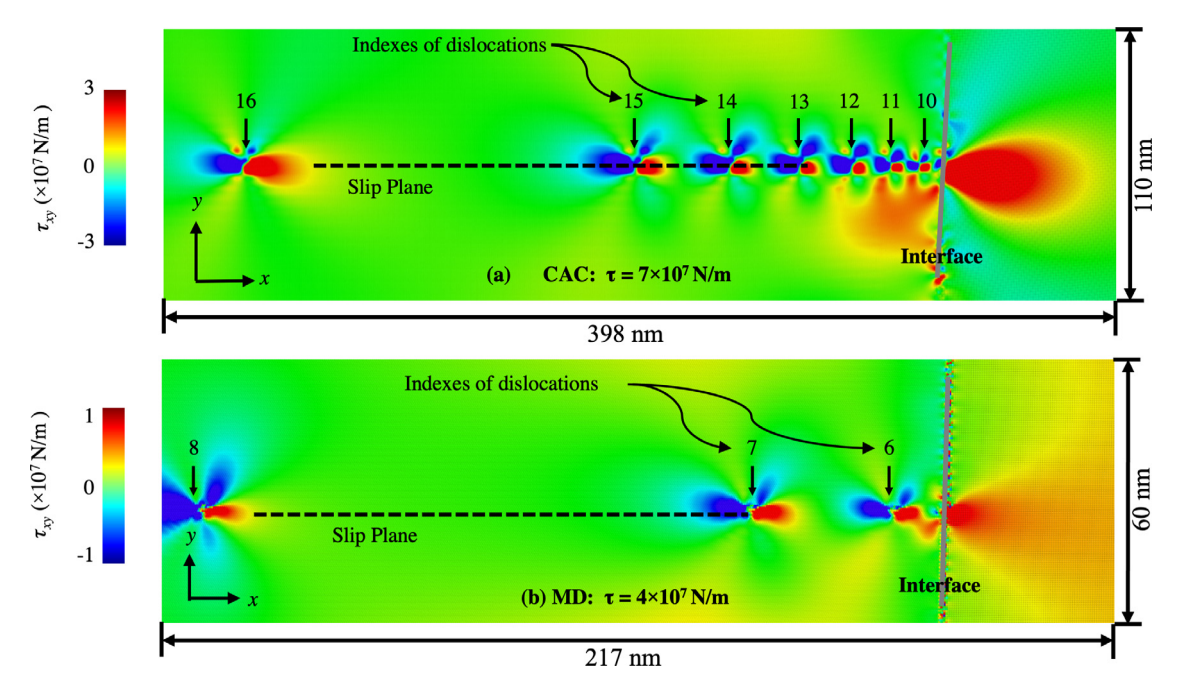


Fig. 3. The atomic - scale structure evolution at the slip - interface intersection when different number of dislocations arrive at the interface in the time sequences, with the formation of the step with a height of 5b when 5 dislocations arrive at the interface under  $\tau_{ap} = 4 \times 10^7$  N/m.



**Fig. 4.** The configuration of the local stress ( $\tau_{xy}$ ) field of dislocations in a pileup from truncated: (a) microscale CAC: 16 dislocations are piled up against the interface under a shear  $\tau_{ap} = 7 \times 10^7$  N/m. 9 of them arrive at the interface; and (b) nanoscale MD: 8 dislocations are piled up at  $\tau_{ap} = 4 \times 10^7$  N/m. 5 of them arrive at the interface.

piled up at the interface no matter how long we run the simulations, which is reported in our separate work [76].

### 3.2. The dislocation pileup process

A retaining of the fully atomistic resolution at the interface provides us with an opportunity of examining the detailed process of a slip-interface reaction. Fig. 3 presents the time sequences of the snapshots showing the reaction between dislocations and the interface at the early stage of the simulations with the atoms being color coded with the coordination number (red: hexagonal; blue: square; other: green). It should be noted that the simulation box shown in Fig. 3 has been truncated to display the atomic structures only at the slip-interface intersection. Fig. 3 a and b shows that, when one dislocation arrives at the interface, a step of 2.56 Å, i.e., the magnitude of one Burgers vector **b**, forms. With a further increase of the applied shear, more dislocations will arrive at the interface and eventually, a step with a larger height will be formed. This step can be approximately considered as a single "super-dislocation" with a Burgers vector of  $N\mathbf{b}$ , with N as the number of dislocations arriving at the interface. Under a shear stress of  $\tau_{ap} = 8 \times 10^7$  N/m, 5 dislocations have arrived at the interface. The "super-dislocation" at the interface has a Burgers' vector of 5b (Fig. 3 c).

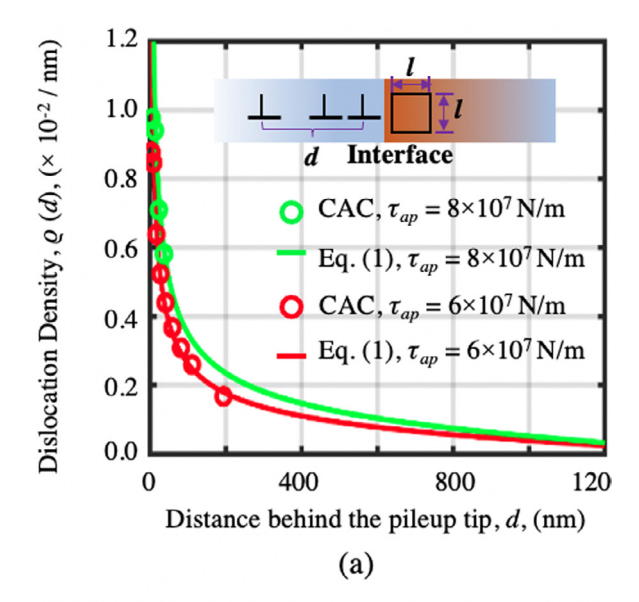
Three major findings from Fig. 3 are: (1) as desired, the interface under consideration here indeed blocks the motion of dislocations without allowing any transmission. This is also the case even when we extend the timescale of the simulations up to several nanoseconds and longer [76]; (2) CAC resolves the fully atomistic details of a slip-interface reaction; and (3) a step-like "superdislocation" with a complex local atomistic structure is formed at the slip-interface intersection. Similar features were observed in our previous three-dimensional MD simulations of dislocation pileup against tilt GBs in Si, which caused amorphization [77].

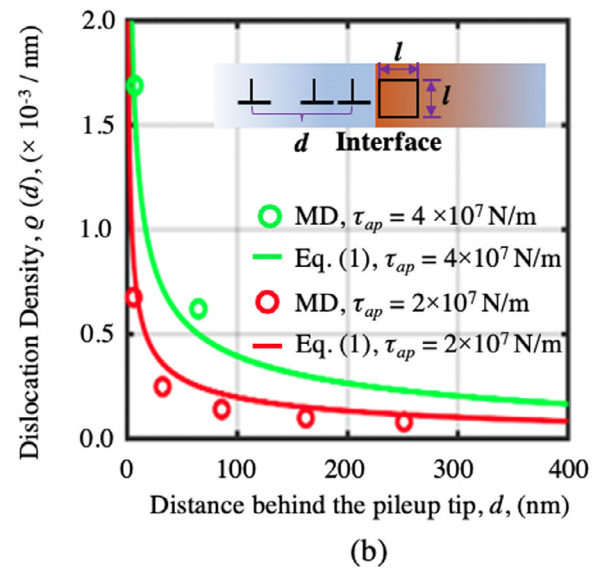
Fig. 4 a and 4 b shows the results from CAC and MD simulations of 16 and 8 dislocations piling up at the interface under a shear stress of  $\tau_{ap} = 7 \times 10^7$  N/m and  $\tau_{ap} = 4 \times 10^7$  N/m, respectively. It should be pointed out that, since all the dislocations are initially indexed before any external shear is imposed, dislocations 1–9 in

Fig. 4 a and dislocations 1-5 in Fig. 4 b are gone because they have fully arrived at the interface and formed a step there. The heights of the steps in Fig. 4 a and 4 b are 9b and 5b, respectively. It is seen that: (i) Dislocations in CAC smoothly migrate from the CG to the atomistically resolved interface domain; (ii) The pileup can form at the interface without the occurrence of any transmission in both MD and CAC; (iii) The dislocation transmission is not observed even we significantly increase the timescale of the simulation run up to several nanoseconds; and (iv) A square-to-hexagonal PT is observed in such long-run simulations as reported elsewhere [76]. Several main observations from Fig. 4 a and b are: (1) The local shear stress field,  $\tau_{xy}$ , around a single dislocation far away from the interface, such as the 16th dislocation in Fig. 4 a and the 8th dislocation in Fig. 4 b, is comparable with the solution from the theory of elasticity. In contrast,  $\tau_{xy}$  around the dislocations close to the pileup tip, such as the 10th-12th dislocations in Fig. 4 a and the 6th dislocation in Fig. 4 b, has been largely altered. This is believed to be correlated with the atomic-level structure distortion at the slip-interface intersection; and (2) A stress concentration has been generated ahead of the pileup tip in both CAC and MD. According to the results obtained from CAC (Fig. 4 a), this stress concentration spans a length scale at a range of 130 nm and will be even longer if more dislocations are included in the pileup. A full MD simulation at this length scale will be computationally demanding, if not impossible. In our current MD models with a limited space (70 nm) between the pileup tip and the free end of the sample, the stress concentration ahead of the dislocation pileup tip has been largely released due to the presence of the free surface (Fig. 4 b), although only 8 dislocations have participated in the pileup there.

### 3.3. The dislocation configuration in a pileup

Here, for comparison, the computer simulation-predicted dislocation configuration in a pileup is compared with results from the Eshelby model [46]. According to this model, the distribution of a continuous dislocation density (noted as  $\rho(d)$ , i.e., the number of dislocations per unit length) behind the pileup tip approximately





**Fig. 5.** (a) CAC and (b) MD simulation-predicted  $\rho(d)$  as a function of the distance, d, behind the tip of a pileup at the interface and its comparison with continuum solutions. Here,  $\rho(d)$  is only for dislocation density behind the pileup tip and does not include the dislocations that have formed the step on the interface.

obeys:

$$\rho(d) = \frac{2(1-\nu)\tau_{ap}}{\mu b} \cdot \frac{L_{x-\text{hex}} - d}{\sqrt{L_{x-\text{hex}}^2 - (L_{x-\text{hex}} - d)^2}},$$
 (4)

where d is the distance away from the tip of a pileup (see the indication of d in the inset pictures of Fig. 5 a and b);  $\tau_{ap}$  is the applied shear stress;  $\mu$  is the shear modulus of the materials containing dislocations, i.e., the hexagonal lattice here; b is the Burgers vector of dislocations; v is Poisson's ratio of the material. In this work,  $\mu = 35.4 \times 10^7$  N/m, b = 2.56 Å, and v = 0.3. Before comparing our simulation results with Eshelby solutions, we would like to point out that the derivation of Eq. (4) is under several key assumptions: (i) it is a mathematical treatment under a continuum approximation based on the theory of linear isotropic elasticity and has ignored the dislocation core structures; (ii) the obstacle acting as a barrier to dislocation's motion in Eshelby model is assumed to be fully rigid. It does not allow any local relaxation at the dislocation pileup tip; and (iii) the Eshelby model does not take any free

surface-induced image stresses into account by considering dislocations embedded within an infinite medium.

Fig. 5 a and 5 b shows the CAC- and MD-simulation-predicted dislocation density distributions behind the pileup tip and their comparison with that from Eq. (4), respectively. Here,  $\rho(d)$  is estimated by directly counting the number of dislocations per unit length within a distance, d, away from the pileup tip.  $\rho(d)$  shown in Fig. 5 a and b does not include any dislocations that have participated the formation of the steps on the interface. Several key findings from Fig. 5 a and b are: (a) the density of dislocation distribution,  $\rho(d)$ , especially  $\rho(d)$  near the tip at  $d \to 0$ , significantly increases with the increase of applied shear stress. This is consistently observed in CAC, MD, as well as Eq. (4); (b) the CACsimulation-predicted dislocation density distribution under  $\tau_{ap}$  =  $6 \times 10^7$  N/m and  $\tau_{ap} = 8 \times 10^7$  N/m agrees perfectly well with that from Eq. (4) (Fig. 5 a), especially when d > 20 nm, although the assumption of linear isotropy has been deployed in the Eshelby model but anisotropy is retained in CAC; (c) at  $\tau_{ap} = 8 \times 10^7$  N/m, different from the singularity predicted by Eshelby for  $\rho(d)$  at  $d \rightarrow$ 0 in Eq. (4), the CAC-predicted  $\rho(d)$  saturates at  $d \to 0$  (Fig. 5 a). This is believed to be reasonable because the CAC model allows a local relaxation at the tip while the Eshelby model has assumed a rigid obstacle; (d) comparing with the results from the microscale CAC simulations, the dislocation density distribution from MD (Fig. 5 b) also agrees reasonably well with that from Eq. (4) even at  $d \rightarrow$ 0. Because  $\tau_{ap}$  applied on the MD model is lower than that in CAC, at this stress level, the local structure at the pileup tip does not relax and the interface may be still approximately considered as a rigid obstacle; and (e) when 16 dislocations participate the pileup formation, at  $\tau_{ap}=8\times10^7$  N/m,  $\rho(d)$  does not decay to zero at d=1.2  $\mu m$  (Fig. 5 a). In contrast, when only 8 dislocations participate in the pileup, (Fig. 5), even at  $\tau_{ap} = 4 \times 10^7$  N/m,  $\rho(d)$  decays to zero at d=0.4 µm. This result suggests that the pileup containing tens of or more dislocations spans a length scale at the micrometer level or above, which can be captured by CAC but is beyond the reach of a full MD model, if a modest computational resource is used.

### 3.4. The dislocation pileup-induced stress concentration

In addition to dislocation density distribution, the CAC- and MD-simulation-predicted stress distribution, especially the stress profile, ahead of the pileup tip is also characterized. To measure the local stress, in both CAC and MD models, a series of finite-sized volume elements are constructed ahead of the pileup tip, each of which is in a high resolution with a dimension of 5 Å  $\times$  5Å and contains approximately four atoms. Then the stress tensor associated with each volume element is calculated using a Virial formula [78]. In this way, the dislocation pileup-induced stress profile ahead of the slip-interface intersection can be determined. We are aware that the deployment of a Virial formula for measuring the local stress in an atomistic system may not be precise due to its inconsistency with the definition of continuum-level Cauchy stress [79]. A measurement of the local stress using the newly developed atomic-level Cauchy stress formula in [80] is not used here but will be attempted in our future work. The obtained stress profiles are then fitted into an Eshelby-type model, i.e., Eq. (5), which is a generalization of the classical Eshelby model [46] by introducing an additional parameter, a, into it (a = 0.5 in classical Eshelby model). Two major reasons for such a generalization are: (a) the local stress' decay as a function of  $1/r^{0.5}$  (here r is the the distance away from the slip-interface intersection) in the classical Eshelby model is built upon an assumption on treating the dislocation barrier as a rigid obstacle, which is obviously not the case here; (b) the step formation at the slip-interface intersection is accompanied by a complex local structure evolution, which may have led

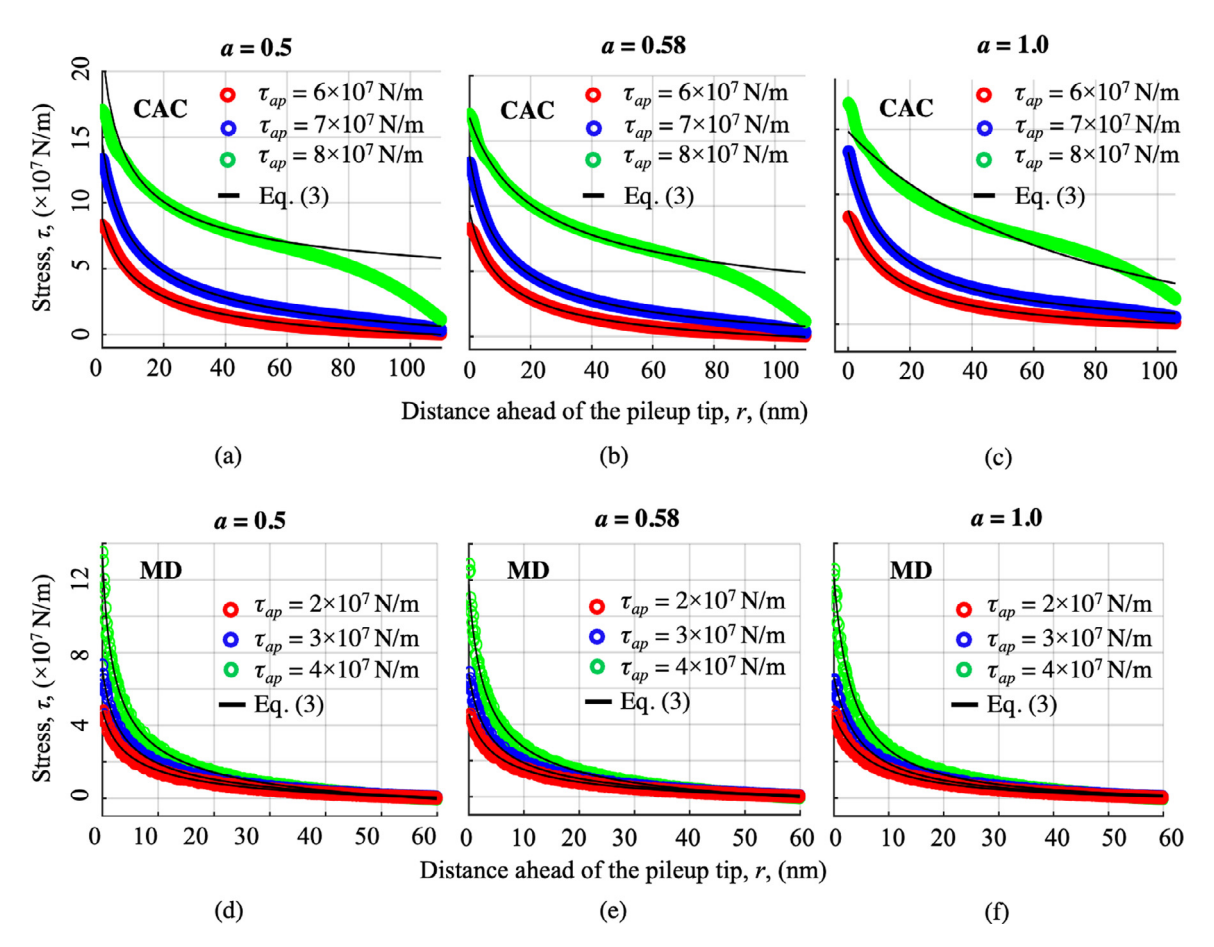


**Fig. 6.** The local stress profile ahead of the slip-interface intersection along the slip direction under a variety of  $\tau_{ap}$  from CAC and MD simulations and their fits into Eq. (5), the extended Eshelby model with (a,d) a=0.5, (b,e) a=0.58, (c,f) a=1.

to a stress redistribution deviating from  $1/r^{0.5}$ , especially when a large number of dislocations arrive at the interface. Under this argument, a generalized Eshelby model for characterizing the stress profile, e.g.,  $\tau$ , ahead of the pileup tip is proposed as:

$$\tau = \tau_0 + \frac{K}{(r + r_0)^a},\tag{5}$$

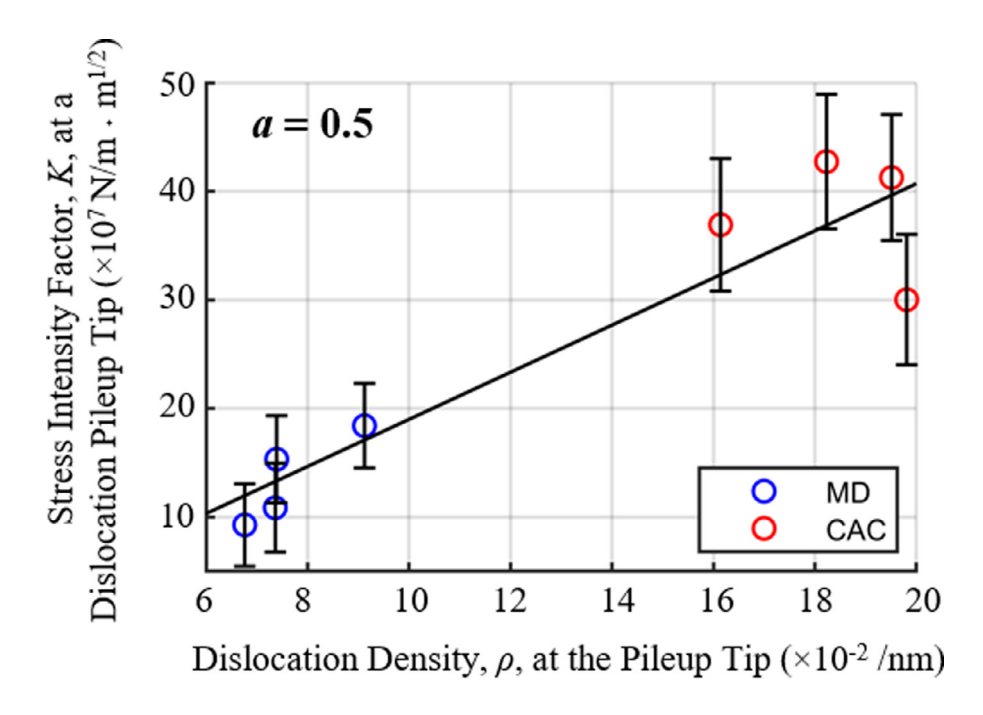
where  $\tau$  is the local shear stress ahead of the pileup tip, K is the stress intensity factor at the pileup tip, and r is the distance between the pileup tip and the stress measurement site (the center of the volume element in the inset picture of Fig. 5). Two parameters,  $\tau_0$  and  $r_0$ , in Eq. (5) account for the uncertainty associated with the reference stress state and the location of the pileup tip, respectively. The parameter a is introduced here to accommodate the local structure relaxation at the slip-interface intersection.

Fig. 6 presents the MD- and CAC-simulation-predicted shear stress distributions ahead of the dislocation pileup tip, as well as their fits into the Eshelby-type model at three typical values of a. Several major findings here are:

(a) Both CAC (Fig. 6 a–c) and MD (Fig. 6 d–f) data fit into Eq. (5) predicting an exponential decay of  $\tau$  ahead of the dislocation pileup tip. One common feature between CAC and MD simulations are: the stress level as well as the stress range ahead of the pileup tip will be amplified when the applied shear stress,  $\tau_{ap}$ , is increased because the number of dislocations arriving at the interface becomes more at a higher  $\tau_{ap}$ . In details, when the applied shear stress is relatively low but increases from  $2\times10^7$  N/m (red curves in Fig. 6 d–f) to  $4\times10^7$  N/m (green curves in Fig. 6 d–f), the local stress at the pileup tip (r=0) increases from  $4\times10^7$  N/m to  $14\times10^7$  N/m. This stress concentration does not decay to zero un-

til r=20 nm and r=40 nm when  $\tau_{ap}=2\times10^7$  N/m and  $\tau_{ap}=4\times10^7$  N/m, respectively. Upon a further  $\tau_{ap}$  increase from  $6\times10^7$  N/m (red curves in Fig. 6 a–c) to  $8\times10^7$  N/m (green curve in Fig. 6 a–c), the stress concentration at the pileup tip (r=0) increases up to  $17\times10^7$  N/m. At this stage, the number of dislocations participating the pileup is 16, which can not be accommodated by the current MD models. Thus, all the results in Fig. 6 a–c are obtained from CAC simulations. Obviously, the participation of a large number of dislocations in the pileup produces a long-range stress profile spanning hundreds of nanometers (Fig. 6 a–c), which does not decay to zero until the free surface at r=138 nm. We believe that, similar to what has been observed in experiments [81], such a slip-interface interaction-induced stress concentration can span tens of microns as long as more dislocations are included into the pileup in an even larger sample by CAC.

**(b)** When the applied shear stress,  $\tau_{ap}$ , is  $7\times10^7$  N/m and below, all the CAC and MD simulation data fit into Eq. (5) perfectly well no matter what value has been chosen for a. However, when  $\tau_{ap}$  is increased up to  $8\times10^7$  N/m (green curves in Fig. 6 a–c), the simulation data differs from Eq. (5) in two main aspects. Firstly, Eq. (5) still predicts a finite stress even at r=138 nm, which should be zero due to the presence of a free surface there. Because the Eshelby model is formulated for the stress field induced by a pileup buried in an infinite medium, it does not consider the relaxation induced by a free surface and thus predicts a finite stress at a level of  $5\times10^7$  N/m at r=138 nm when  $\tau_{ap}=8\times10^7$  N/m. In contrast, under  $\tau_{ap}=8\times10^7$  N/m, a zero stress at r=138 nm has been naturally captured by CAC simulations (green curves in Fig. 6 a–c). Secondly, when a=0.5 (Fig. 6 a) or a=1.0 (Fig. 6 c),



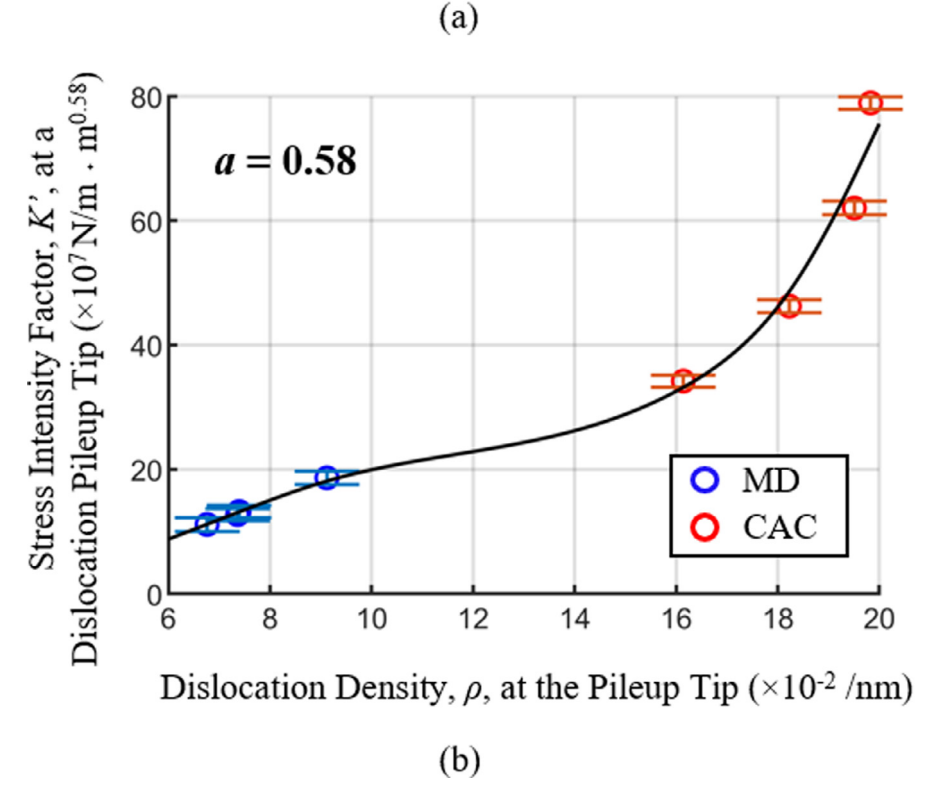
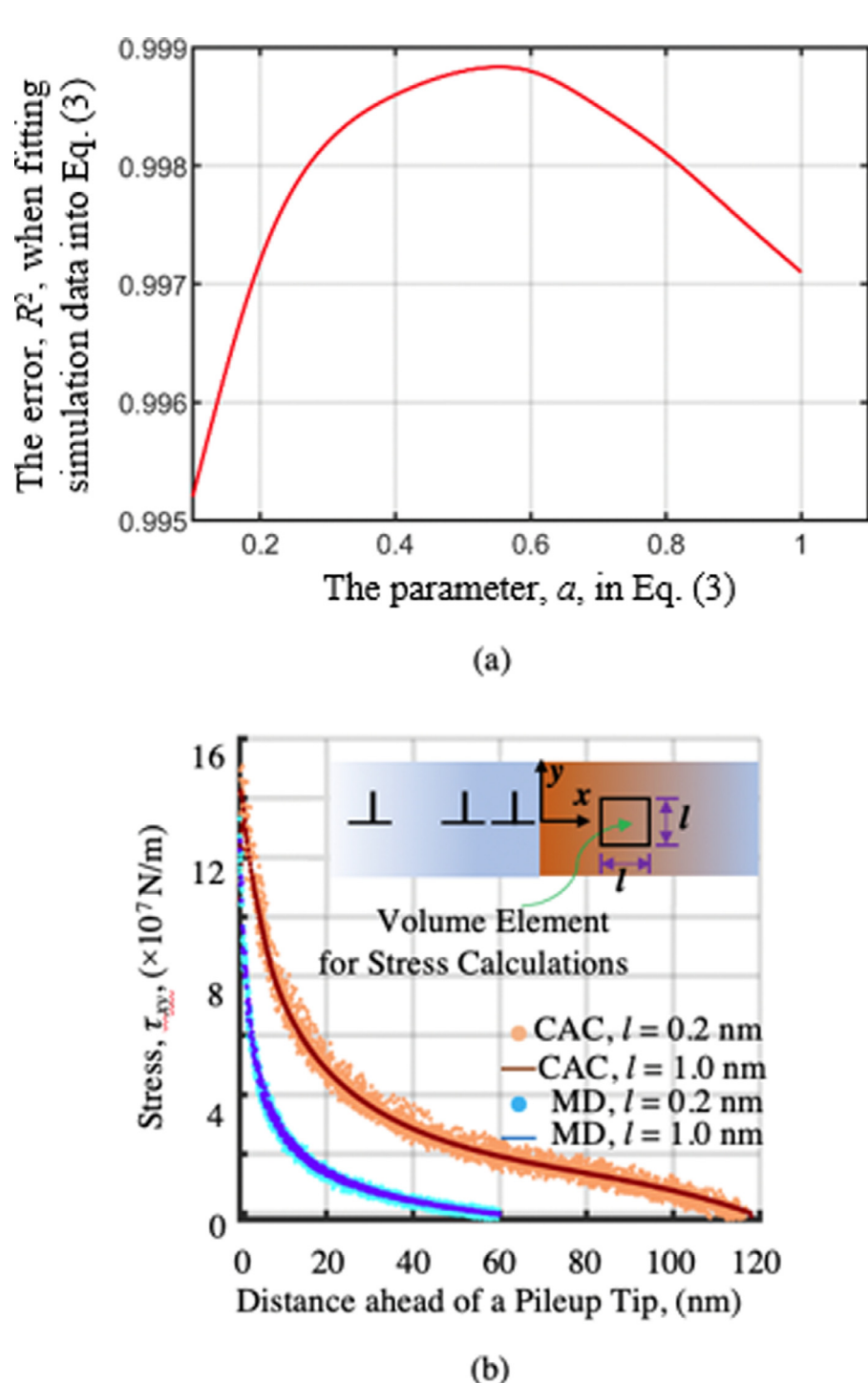


Fig. 7. The relation between the fitted stress intensity factor K and the density of dislocations  $\rho^*$  at the interface when setting (a) a = 0.5 and (b) a = 0.58.

at the site very close to the pileup tip, i.e.,  $r \to 0$ , the stress concentrations from CAC simulations deviate from Eq. (5). In particular, simulation data shows that  $\tau_{r\to 0}$  is  $17\times 10^7$  N/m at  $\tau_{ap}$  is  $8\times 10^7$  N/m, which is lower than that  $(\tau_{r\to 0}\ 20\times 10^7\ \text{N/m})$  from Eq. (5) when a=0.5, but is higher than that from Eq. (5) when  $a=1\ (\tau_{r\to 0}\ 15\times 10^7\ \text{N/m})$ . For either a=0.5 (Fig. 6 a) or a=1.0 (Fig. 6 c), such differences between simulation data and the prediction from from Eq. (5) can even amplify if  $\tau_{ap}$  further increases.

The obtained results then lead to two plots with the  $K-\rho^*$  relation as shown in Fig. 7. In details, the vertical axis of Fig. 7 a

and 7 b indicates the fitted stress intensity factor, K, when setting a=0.50 and a=0.58, respectively. Here, the error bar is induced by the resolution-dependence of the local stress measurements. For a=0.5 and a=0.58, the stress intensity factor K ahead of the pileup tip is measured through the fitting of Eq. (5) and correlated with the density of dislocations,  $\rho^*$ , accumulated near the interface. Fig. 7 shows that, for both a=0.5 and a=0.58, consistent with previous MD simulation results in [82], the stress intensity factor, K, ahead of a pileup is proportional to the density of dislocations accumulated at the interface. For a=0.5, the stress intensity



**Fig. 8.** (a) the numerical error,  $R^2$ , when fitting simulation data into Eq. (5) and its dependence on the choice of fitting parameter of a; (b) the resolution dependence of local stress profile ahead of the slip-interface intersection in CAC and MD simulations.

sity linearly increases with the increase of the dislocation density (Fig. 7 a) and then suddenly drops at  $\rho^*(d){=}19{\times}10^{-2}$  /nm, corresponding to which the number of dislocations in the pileup is 16. In contrast, the  $K-\rho^*$  relation in Fig. 7 b at a=0.58 is highly nonlinear and behaves significantly different from that in Fig. 7 a. In Fig. 7 b, K sharply increases at  $\rho^*(d){=}19{\times}10^{-2}$  /nm, instead of the sudden drop as shown in Fig. 7 a where a=0.5. Obviously, such results cannot be simply obtained by MD simulations alone because MD simulation will always only predict a linear  $K-\rho^*$  relation by only accommodating several dislocations in a pileup. This can be evidenced by the blue circle data points in Fig. 7 a and b.

Such an atomic-to-microscale simulation-based K- $\rho^*$  relation may be used to interpret results from microscale experiments, such as [83], where the dislocation density  $\rho^*$  near a GB and the dislocation pileup-induced stress concentration has been measured. However, a quantitative connection between simulations and experiments needs to be taken with great caution because the measurement of K in both experiments and simulations involves a considerable uncertainty. In particular, the K values from CAC and MD obviously depends on the resolution to be deployed in the local stress measurement. In both CAC and MD, a significant fluctuation appears in the pileup-induced stress profile if different resolutions

(noted as l) are used in measuring the local stress (Fig. 7 b). For instance, the error bar induced by the numerical fitting at a=0.58 is significantly narrower than that of a=0.5. It means that the relaxation of the parameter of a largely suppresses the uncertainty in determining the stress intensity factor of K. Such uncertainties cannot be ignored despite the overall trend of the  $K-\rho^*$  relation remain unchanged at different a.

As a preliminary search of the best fitting parameter a in Eq. (5), Fig. 8 also presents the change of the fitting error,  $R^2$ , upon the variation of the parameter of a from 0 to 1 at a step of 0.01. In details, the expression of the fitting error,  $R^2$ , is defined as,

$$R^2 = 1 - \frac{SS_{res}}{SS_{tot}},\tag{6}$$

where  $SS_{tot}$  is the total sum of squares  $\sum_i (\sigma_i - \bar{\sigma})$ , and  $SS_{res}$  is the residual sum of squares  $\sum_i (\sigma_i - f_i)^2$ .  $\sigma_i$  is the stress on each volume element,  $\bar{\sigma}$  is the mean of the data points, and  $f_i$  is the fitted value. By this definition, a value of  $R^2$  closer to 1 implies a less error when fitting simulation data into Eq. (5).

Results in both Figs. 6 b, 6 e, and 8 a show that a choice of a =0.58 leads to a best fit of simulation data into Eq. (5). It should be pointed out that, a = 0.58 is simply determined by maximizing  $R^2$ . Although a = 0.58 may not be a typical value, we believe that its deviation from 0.5 or 1 is physically reasonable in general because a = 0.5 corresponds to the dislocation pileup at an ideally rigid interface without any step formation while a = 1.0 corresponds to the formation of a "perfect" step at the pileup tip without any local structure relaxation. This finding implies that the pileup-induced stress concentration indeed decays away from the pileup tip in a similar trend as that in Eshelby model, but decays more slowly and spans a longer range than what has been predicted by the Eshelby model. In other words, although a continuum-level Eshelbytype model can approximately describe the pileup-induced internal stresses, it, however, has a limited resolution because it smears out the step formation and any other local structure relaxation at the slip-interface intersection. In order to further confirm that a best fit of simulation data into Eq. (5) has been achieved at a = 0.58 indeed no matter what resolution has been employed in the stress measurement, Fig. 8b presents the simulation-based stress profiles at different resolutions and their fits into Eq. (5). It is seen that, with the volume element size (noted as l, the side length of one volume element) being decreased from l = 1.0 nm to l = 0.2 nm, the local stress profile exhibits a notable fluctuation but still obeys the Eshelby-type model very well.

The above results suggest: **(1)** CAC simulations not only reproduce a  $K-\rho^*$  relation, which is consistent with the prediction from nanoscale MD simulations in [82], but also expand the predictive capability of MD simulations up to the microscale by accommodating tens of dislocations in a pileup; **(2)** this in turn enables CAC to capture the long-range stress field caused by the accumulation of a large number of dislocations at a buried interface. With a unique feature of simultaneously resolving the long-range stress field together with an atomic-level structure evolution at the slip-interface intersection, CAC bridges the length scale gap between atomistic and continuum, and provides us with a platform for simulating dislocation slip, PTs, twinning, and their interactions discussed in details elsewhere [76].

## 4. Summary and discussion

To summarize, in this work, we present atomistic-to-micoscale computational analysis of the local stress complexity induced by the dislocation pileup at an interface in two-phase materials under a plastic shear. One main novelty of the CAC approach deployed here is its capability in bridging the relevant length scales by resolving the atomic-level structure changes near a buried material

interface while the lagging dislocations away from the interface in a coarse-grained atomistic description. It thus expands the MD-simulation-based predictive capability from the nanoscale to the micrometer level. This can be evidenced by our several main findings as follows:

- (1) The CAC model accommodates up to 16 dislocations in one slip at a modest computational cost. Under certain shear stresses, these dislocations may be blocked by obstacles (an incoherent interface in this work) and form a pileup spanning a range of several micrometers (1.2  $\mu m$  in the present model). In contrast, the MD model using the same computational resource can only accommodate up to 8 dislocations in a pileup, the equilibrium configuration of which under certain shear stress only spans a range of tens or hundreds of nanometers.
- **(2)** When tens of dislocations are piled up at the interface, the CAC-simulation-predicted stress concentration ahead of the pileup tip is also in a long-range. It does not decay to zero at a site hundreds of nanometers away from the pileup tip. This range can be even longer if more dislocations are introduced. This is also confirmed in our recent microscale CAC simulation of the dislocation pileup in Ti-alloys to be reported in [84]. In contrast, the MD-simulation-predicted stress concentration ahead the tip of a pileup containing a few dislocations spans only 60 nm.
- (3) When the number of dislocations in a pileup is as small as considered in MD, or when the number of dislocations participating in the pileup is large but the applied stress is relatively low, the continuum-level Eshelby model [46] predicts well about the dislocation density,  $\rho$ , behind a pileup and also the stress intensity, K, ahead of a pileup tip. In such situations, an increase of  $\rho$  and K with the increase of  $\tau_{ap}$  is consistently observed in MD, CAC, and the Eshelby-type models.
- (4) When the number of dislocations in a pileup increases up to 16, under a high shear stress, CAC predicts a pileup-induced step formation at the interface, a considerable stress concentration ahead of the pileup tip, a saturation of the dislocation density,  $\rho^*$ , behind the pileup tip, and most importantly, a sudden "upper bend" of the pileup tip stress intensity factor, K, up to a very high level. At this stage, our two main observations contradicting to the conventional wisdom are: (a) the stress profile ahead of the pileup tip obeys neither  $1/r^{0.5}$  (the classical Eshelby model, assuming a rigid obstacle without allowing the step formation at the interface) nor 1/r (the superposition model, assuming the formation of a perfect step without any local structure relaxation at the interface); (b) the relationship between the local stress intensity factor and the dislocation density near the interface, i.e., the  $K-\rho^*$  relation, is not as linear as reported by many existing MD simulations which only consider a few dislocations piling up at the obstacles, but is highly non-linear instead. A simple linear correlation between dislocation density and the stress intensity factor may have largely underestimated the dislocation accumulation-induced local stress intensity within the materials.

These findings highlight: **(a)** the insufficiency of only using nanoscale MD simulations to interpret the microscale experimental results on such phenomenon, which may have involved tens and even hundreds of µm-long dislocations; **(b)** the need for a multiscale materials modeling methodology to bridge the length scale gap between atomistic simulations, experiments, and continuum-level approaches for the problem under consideration; and **(c)** the possibility of engineering the microstructure of a plastically deformed two-phase materials, such as fcc/bcc, fcc/hcp, bcc/hcp metallic composites, Ti-/Zr-/high entropy alloys, and among several others, through a fine control of the microscale dislocation-mediated plastic flow and its interaction with the buried material interfaces through multiscale computer simulations.

The results that we have presented here suggest that the CAC simulation tool may provide researchers with an alternative vehicle

to meet this need, but are considered to be still preliminary at this stage because:

- (i) the material system under consideration here is simplified in terms of crystal structure, chemistry, interatomic potential, microstructure and among several others. A transfer of the present model or the gained knowledge for understanding the slip-interface reactions in realistic multiphase material is not trivial. It demands the design of new finite elements for simultaneously accommodating complex dislocation activities, the implementation of more sophisticated or machine learning-based interatomic potential trained from *ab initio* data for capturing more complex structure changes, as well as the incorporation of realistic structures and chemistry at the GBs, PBs, and other interfaces in the materials.
- (ii) in addition to the local stress, another factor that plays a vital role in the local structural change is the thermal-induced atomic fluctuations. The implementation of a finite temperature algorithm into CAC for capturing the thermal effects on dislocations, PTs, and their interactions is needed, especially when the correlation between phonon instability and PTs becomes a concern.
- (iii) The critical applied stress at which the step forms at the interface may have been overestimated due to the limitation of simulation timescale in MD and CAC. Since the structural change of interest can be many orders of magnitude slower than the vibrations of the atoms, conventional MD or CAC is not able to quantitatively capture the realistic atomic structure revolution that is observed in experimental time scale. The nudged elastic band (NEB) methods have been generally used to determine the atomic structure revolution of such long time scale event. In particular, a finite deformation NEB method was recently developed to determine the stress dependent minimum energy path of a phase transition under finite deformation [85], which has been applied to study the PTs in 2D materials [45] and silicon [86]. Although NEB methods could help resolve the challenges from the time scale, it still faces the challenges in the length scales. To this end, an integration of CAC and NEB methods is promising to further push the predictive capability of atomistic simulations by resolving the large length and time scales simultaneously.

A further expansion of CAC along with the above three directions and its applications in predicting the slip-interface reactions in a variety of realistic materials are being intensively pursued in our group. The relevant results will be reported in our future publications.

### **Declaration of Competing Interest**

The authors declare that they have no known competing financial interests or personal relationships that could have appeared to influence the work reported in this paper.

### Acknowledgments

YP, RJ, TP, and LX acknowledge the support of the U.S. National Science Foundation (DMR-1807545 and CMMI-1930093) and the Extreme Science & Engineering Discovery Environment (XSEDE-TG-MSS170003, XSEDE-TG-MSS190008 and XSEDE-TG-MSS190013). WG gratefully acknowledge the support of the U.S. National Science Foundation through Grant no. CMMI-1930783. VIL work was funded by NSF (MMN-1904830 and CMMI-1943710), ONR (N00014-16-1-2079), and the ISU (Vance Coffman Faculty Chair Professorship), as well as XSEDE, allocation TG-MSS170015.

## References

[1] Y. Guo, T.B. Britton, A.J. Wilkinson, Slip band–grain boundary interactions in commercial-purity titanium, Acta Mater. 76 (2014) 1–12.

[2] D.C. Johnson, B. Kuhr, D. Farkas, G.S. Was, Quantitative linkage between the stress at dislocation channel-Grain boundary interaction sites and irradiation assisted stress corrosion crack initiation, Acta Mater. 170 (2019) 166– 175.

- [3] T.C. Lee, I.M. Robertson, H.K. Birnbaum, An in situ transmission electron microscope deformation study of the slip transfer mechanisms in metals, Metall. Trans. A 21 (9) (1990) 2437–2447.
- [4] J. Kacher, I.M. Robertson, Quasi-four-dimensional analysis of dislocation interactions with grain boundaries in 304 stainless steel, Acta Mater. 60 (19) (2012) 6657–6672
- [5] J.B. Singh, G. Molénat, M. Sundararaman, S. Banerjee, G. Saada, P. Veyssière, A. Couret, In situ straining investigation of slip transfer across α2 lamellae at room temperature in a lamellar TiAl alloy, Philos. Mag. Lett. 86 (1) (2006) 47–60
- [6] V.I. Levitas, High-pressure mechanochemistry: conceptual multiscale theory and interpretation of experiments, Phys. Rev. B 70 (18) (2004) 184118.
- [7] P.M. Anderson, J.P. Hirth, J. Lothe, Theory of Dislocations, Cambridge University Press, 2017.
- [8] T.R. Bieler, S.C. Sutton, B.E. Dunlap, Z.A. Keith, P. Eisenlohr, M.A. Crimp, B.L. Boyce, Grain boundary responses to heterogeneous deformation in tantalum polycrystals, J. Mater. 66 (1) (2014) 121–128.
- [9] L. Wang, Y. Yang, P. Eisenlohr, T.R. Bieler, M.A. Crimp, D.E. Mason, Twin nucleation by slip transfer across grain boundaries in commercial purity titanium, Metall. Mater. Trans. A 41 (2) (2010) 421.
- [10] A.J. Wilkinson, E.E. Clarke, T.B. Britton, P. Littlewood, P.S. Karamched, High-resolution electron backscatter diffraction: an emerging tool for studying local deformation, J. Strain Anal. Eng. Des. 45 (5) (2010) 365–376.
- [11] W. Clark, R.H. Wagoner, Z.Y. Shen, T.C. Lee, I.M. Robertson, H.K. Birnbaum, On the criteria for slip transmission across interfaces in polycrystals, Scr. Metall. Mater. 26 (2) (1992) 203–206.
- [12] T.C. Lee, I.M. Robertson, H.K. Birnbaum, Interaction of dislocations with grain boundaries in Ni<sub>3</sub>Al, Acta Metall. Mater. 40 (10) (1992) 2569–2579.
- [13] T.C. Lee, I.M. Robertson, H.K. Birnbaum, TEM in situ deformation study of the interaction of lattice dislocations with grain boundaries in metals, Philos. Mag. A 62 (1) (1990) 131–153.
- [14] M. Chassagne, M. Legros, D. Rodney, Atomic-scale simulation of screw dislocation/coherent twin boundary interaction in Al, Au, Cu and Ni, Acta Mater. 59 (4) (2011) 1456–1463.
- [15] Z.-H. Jin, P. Gumbsch, K. Albe, E. Ma, K. Lu, H. Gleiter, H. Hahn, Interactions between non-screw lattice dislocations and coherent twin boundaries in facecentered cubic metals, Acta Mater. 56 (5) (2008) 1126–1135.
- [16] M. De Koning, R.J. Kurtz, V.V. Bulatov, C.H. Henager, R.G. Hoagland, W. Cai, M. Nomura, Modeling of dislocation-grain boundary interactions in FCC metals, J. Nucl. Mater. 323 (2-3) (2003) 281–289.
- [17] S.S. Quek, Z. Wu, Y.W. Zhang, D.J. Srolovitz, Polycrystal deformation in a discrete dislocation dynamics framework, Acta Mater. 75 (2014) 92–105.
- [18] J. Wang, Atomistic simulations of dislocation pileup: grain boundaries interaction, J. Mater. 67 (7) (2015) 1515–1525.
- [19] B.A. Szajewski, W.A. Curtin, Analysis of spurious image forces in atomistic simulations of dislocations, Model. Simul. Mater. Sci. Eng. 23 (2) (2015) 025008.
- [20] Y. Peng, L. Xiong, Atomistic computational analysis of the loading orientation-dependent phase transformation in graphite under compression, J. Mater. 71 (11) (2019) 3892–3902.
- [21] S. Puri, A. Acharya, A.D. Rollett, Controlling plastic flow across grain boundaries in a continuum model, Metall. Mater. Trans. A 42 (3) (2011) 669–675.
- [22] J.R. Mayeur, I.J. Beyerlein, C.A. Bronkhorst, H.M. Mourad, Incorporating interface affected zones into crystal plasticity, Int. J. Plast. 65 (2015) 206–225.
- [23] X. Zhan, A continuum model for dislocation pile-up problems, Acta Mater. 128 (2017) 428–439.
- [24] V.A. Lubarda, A pileup of edge dislocations against an inclined bimetallic interface, Mech. Mater. 117 (2018) 32–40.
- [25] M. Javanbakht, V.I. Levitas, Phase field approach to dislocation evolution at large strains: computational aspects, Int. J. Solids Struct. 82 (2016) 95–110.
- [26] V.I. Levitas, M. Javanbakht, Phase field approach to interaction of phase transformation and dislocation evolution, Appl. Phys. Lett. 102 (25) (2013) 251904.
- [27] M. Javanbakht, V.I. Levitas, Nanoscale mechanisms for high-pressure mechanochemistry: a phase field study, J. Mater. Sci. 53 (19) (2018) 13343–13363.
- [28] L. Xiong, Q. Deng, G. Tucker, D.L. McDowell, Y. Chen, A concurrent scheme for passing dislocations from atomistic to continuum domains, Acta Mater. 60 (3) (2012) 899–913.
- [29] L. Xiong, S. Xu, D.L. McDowell, Y. Chen, Concurrent atomistic-continuum simulations of dislocation-void interactions in FCC crystals, Int. J. Plast. 65 (2015) 33-47
- [30] S. Xu, L. Xiong, Y. Chen, D.L. McDowell, Sequential slip transfer of mixed-character dislocations across Σ3 coherent twin boundary in FCC metals: a concurrent atomistic-continuum study, npj Comput. Mater. 2 (1) (2016) 1–9.
- [31] L. Xiong, D.L. McDowell, Y. Chen, Nucleation and growth of dislocation loops in Cu, Al and Si by a concurrent atomistic-continuum method, Scr. Mater. 67 (7-8) (2012) 633-636.
- [32] S. Xu, L. Xiong, Q. Deng, D.L. McDowell, Mesh refinement schemes for the concurrent atomistic-continuum method, Int. J. Solids Struct. 90 (2016) 144–152.
   [33] L. Xiong, X. Chen, N. Zhang, D.L. McDowell, Y. Chen, Prediction of phonon prop-
- [33] L. Xiong, X. Chen, N. Zhang, D.L. McDowell, Y. Chen, Prediction of phonon properties of 1D polyatomic systems using concurrent atomistic-continuum simulation, Arch. Appl. Mech. 84 (9) (2014) 1665–1675.

- [34] S. Xu, T.G. Payne, H. Chen, Y. Liu, L. Xiong, Y. Chen, D.L. McDowell, PyCAC: the concurrent atomistic-continuum simulation environment, J. Mater. Res. 33 (7) (2018) 857.
- [35] H. Chen, S. Xu, W. Li, R. Ji, T. Phan, L. Xiong, A spatial decomposition parallel algorithm for a concurrent atomistic-continuum simulator and its preliminary applications, Comput. Mater. Sci. 144 (2018) 1–10.
- [36] X. Chen, A. Diaz, L. Xiong, D.L. McDowell, Y. Chen, Passing waves from atomistic to continuum, J. Comput. Phys. 354 (2018) 393–402.
- [37] S. Xu, L. Xiong, Y. Chen, D.L. McDowell, Validation of the concurrent atomistic-continuum method on screw dislocation/stacking fault interactions, Crystals 7 (5) (2017) 120.
- [38] L. Xiong, G. Tucker, D.L. McDowell, Y. Chen, Coarse-grained atomistic simulation of dislocations, J. Mech. Phys. Solids 59 (2) (2011) 160–177.
- [39] L. Xiong, Y. Chen, Coarse-grained simulations of single-crystal silicon, Model. Simul. Mater. Sci. Eng. 17 (3) (2009) 035002.
- [40] Y. Chen, Local stress and heat flux in atomistic systems involving three-body forces, J. Chem. Phys. 124 (5) (2006) 054113.
- [41] Y. Chen, Reformulation of microscopic balance equations for multiscale materials modeling, J. Chem. Phys. 130 (13) (2009) 134706.
- [42] Y. Chen, A. Diaz, Physical foundation and consistent formulation of atomic-level fluxes in transport processes, Phys. Rev. E 98 (5) (2018) 052113.
- [43] F. Cellini, F. Lavini, E. Chen, A. Bongiorno, F. Popovic, R.L. Hartman, R. Dingreville, E. Riedo, Pressure-induced formation and mechanical properties of 2D diamond boron nitride, Adv. Sci. 8 (2) (2021) 2002541.
- [44] Y. Peng, F. Wang, Z. Wang, A.M. Alsayed, Z. Zhang, A.G. Yodh, Y. Han, Two-step nucleation mechanism in solid-solid phase transitions, Nat. Mater. 14 (1) (2015) 101–108.
- [45] A. Ghasemi, W. Gao, Atomistic mechanism of stress modulated phase transition in monolayer MoTe<sub>2</sub>, Extreme Mech. Lett. 40 (2020) 100946.
- [46] J.D. Eshelby, F.C. Frank, F. Nabarro, XLI. The equilibrium of linear arrays of dislocations, Lond. Edinb. Dublin Philos. Mag. J. Sci.s 42 (327) (1951) 351–364.
- [47] N. Sridharan, P. Wolcott, M. Dapino, S.S. Babu, Microstructure and texture evolution in aluminum and commercially pure titanium dissimilar welds fabricated using ultrasonic additive manufacturing, Scr. Mater. 117 (2016) 1–5.
- [48] J. Wang, M. Knezevic, M. Jain, S. Pathak, I.J. Beyerlein, Role of interface-affected dislocation motion on the strength of Mg/Nb nanolayered composites inferred by dual-mode confined layer slip crystal plasticity, J. Mech. Phys. Solids 152 (2021) 104421.
- [49] S. Zheng, I.J. Beyerlein, J.S. Carpenter, K. Kang, J. Wang, W. Han, N.A. Mara, High-strength and thermally stable bulk nanolayered composites due to twin-induced interfaces, Nat. Commun. 4 (2013) 1696.
- [50] Y. Chen, A. Diaz, Local momentum and heat fluxes in transient transport processes and inhomogeneous systems, Phys. Rev. E 94 (2016) 053309.
- [51] Y. Chen, The origin of the distinction between microscopic formulas for stress and cauchy stress, Europhys. Lett. 116 (2016) 34003.
- [52] Y. Chen, A. Diaz, Physical foundation and consistent formulation of atomic-level fluxes in transport processes, Phys. Rev. E 98 (2018) 052113.
- [53] J.G. Kirkwood, The statistical mechanical theory of transport processes I. General theory, J. Chem. Phys. 14 (3) (1946) 180–201.
- [54] J.G. Kirkwood, The statistical mechanical theory of transport processes II. Transport in gases, J. Chem. Phys. 15 (1) (1947) 72–76.
- [55] J.H. Irving, J.G. Kirkwood, The statistical mechanical theory of transport processes. IV. The equations of hydrodynamics, J. Chem. Phys. 18 (6) (1950) 817–829.
- [56] R.J. Bearman, J.G. Kirkwood, Statistical mechanics of transport processes. XI. Equations of transport in multicomponent systems, J. Chem. Phys. 28 (1) (1958) 136–145.
- [57] V.I. Levitas, S.E. Esfahani, I. Ghamarian, Scale-free modeling of coupled evolution of discrete dislocation bands and multivariant martensitic microstructure, Phys. Rev. Lett. 121 (20) (2018) 205701.
- [58] S.E. Esfahani, I. Ghamarian, V.I. Levitas, Strain-induced multivariant martensitic transformations: a scale-independent simulation of interaction between localized shear bands and microstructure, Acta Mater. 196 (2020) 430–443.
- [59] R. Gracie, T. Belytschko, Concurrently coupled atomistic and XFEM models for dislocations and cracks, Int. J. Numer. Methods Eng. 78 (3) (2009) 354–378.
- [60] A. Patra, D.L. McDowell, Crystal plasticity investigation of the microstructural factors influencing dislocation channeling in a model irradiated BCC material, Acta Mater. 110 (2016) 364–376.

- [61] J.R. Mayeur, D.L. McDowell, A comparison of Gurtin type and micropolar theories of generalized single crystal plasticity. Int. J. Plast. 57 (2014) 29-51.
- [62] K.Y. Lee, J.R. Ray, Mechanism of pressure-induced martensitic phase transformations: a molecular-dynamics study, Phys. Rev. B 39 (1) (1989) 565.
- [63] S. Plimpton, Fast parallel algorithms for short-range molecular dynamics, J. Comput. Phys. 117 (1) (1995) 1–19.
  [64] S. Xu, T.G. Payne, H. Chen, Y. Liu, L. Xiong, Y. Chen, D.L. McDowell, PyCAC:
- [64] S. Xu, T.G. Payne, H. Chen, Y. Liu, L. Xiong, Y. Chen, D.L. McDowell, PyCAC: the concurrent atomistic-continuum simulation environment, J. Mater. Res. 33 (2018) 857–871.
- [65] J. Luster, M.A. Morris, Compatibility of deformation in two-phase Ti-Al alloys: dependence on microstructure and orientation relationships, Metall. Mater. Trans. A 26 (7) (1995) 1745–1756.
- [66] Z. Zhao, T.R. Bieler, J. LLorca, P. Eisenlohr, Grain boundary slip transfer classification and metric selection with artificial neural networks, Scr. Mater. 185 (2020) 71–75.
- [67] E. Werner, W. Prantl, Slip transfer across grain and phase boundaries, Acta Metall. Mater. 38 (3) (1990) 533-537.
- [68] T.R. Bieler, R. Alizadeh, M. Peña Ortega, J. Llorca, An analysis of (the lack of) slip transfer between near-cube oriented grains in pure Al, Int. J. Plast. 118 (2019) 269–290.
- [69] R. Alizadeh, M. Peña Ortega, T.R. Bieler, J. LLorca, A criterion for slip transfer at grain boundaries in Al, Scr. Mater. 178 (2020) 408–412.
- [70] R.C. Pond, J.P. Hirth, Defects at surfaces and interfaces, Solid State Phys. 47 (1994) 287–365.
- [71] J.P. Hirth, R.C. Pond, Steps, dislocations and disconnections as interface defects relating to structure and phase transformations, Acta Mater. 44 (12) (1996) 4749–4763.
- [72] J.P. Hirth, R.C. Pond, R.G. Hoagland, X.-Y. Liu, J. Wang, Interface defects, reference spaces and the Frank-Bilby equation, Prog. Mater. Sci. 58 (5) (2013) 749–823.
- [73] J.P. Hirth, R.C. Pond, Compatibility and accommodation in displacive phase transformations, Prog. Mater. Sci. 56 (6) (2011) 586–636.
- [74] J.W. Christian, The Theory of Transformations in Metals and Alloys, Newnes, 2002
- [75] G.B. Olson, M. Cohen, Interphase-boundary dislocations and the concept of coherency, Acta Metall. 27 (12) (1979) 1907–1918.
- [76] Y. Peng, R. Ji, T. Phan, V.I. Levitas, L. Capolungo, L. Xiong, Effect of a micro-scale dislocation pileup on the atomic-scale multi-variant phase transformation and twinning, Phys. Rev. B under review (2021).
- [77] H. Chen, V.I. Levitas, L. Xiong, Amorphization induced by 60° shuffle dislocation pileup against different grain boundaries in silicon bicrystal under shear, Acta Mater. 179 (2019) 287–295.
- [78] D.H. Tsai, The virial theorem and stress calculation in molecular dynamics, J. Chem. Phys. 70 (3) (1979) 1375–1382.
- [79] J. Rigelesaiyin, A. Diaz, W. Li, L. Xiong, Y. Chen, Asymmetry of the atomic-level stress tensor in homogeneous and inhomogeneous materials, Proc. R. Soc. A Math. Phys. Eng. Sci. 474 (2217) (2018) 20180155.
- [80] Y. Chen, The origin of the distinction between microscopic formulas for stress and Cauchy stress, EPL (Europhys. Lett.) 116 (3) (2016) 34003.
- [81] T.B. Britton, A.J. Wilkinson, Stress fields and geometrically necessary dislocation density distributions near the head of a blocked slip band, Acta Mater. 60 (16) (2012) 5773–5782.
- [82] B. Kuhr, D. Farkas, I.M. Robertson, D. Johnson, G. Was, Stress localization resulting from grain boundary dislocation interactions in relaxed and defective grain boundaries, Metall. Mater. Trans. A 51 (2) (2020) 667–683.
- [83] I. Ghamarian, Y. Liu, P. Samimi, P.C. Collins, Development and application of a novel precession electron diffraction technique to quantify and map deformation structures in highly deformed materials—as applied to ultrafine-grained titanium, Acta Mater. 79 (2014) 203–215.
- [84] Y. Peng, R. Ji, T. Phan, S. Xu, L. Capolungo, L. Xiong, An atomistic-to-mesoscale characterization of the complex stress field induced by a reaction between slip and grain boundary in titanium and its connection with experiments, 2021. To be submitted.
- [85] A. Ghasemi, P. Xiao, W. Gao, Nudged elastic band method for solid-solid transition under finite deformation, J. Chem. Phys. 151 (2019) 054110.
- [86] A. Ghasemi, W. Gao, A method to predict energy barriers in stress modulated solid-solid phase transitions, J. Mech. Phys. Solids 137 (2020) 103857.